July 27, 2011

Thermal conductivity reduction through isotope substitution in nanomaterials: predictions from an analytical classical model and nonequilibrium molecular dynamics simulations

Ganesh Balasubramanian, *Virginia Polytechnic Institute and State University*
Ishwar K. Puri, *Virginia Polytechnic Institute and State University*
Michael C. Bohm
Frederic Leroy

Nanoscale

PAPER

Thermal conductivity reduction through isotope substitution in nanomaterials: predictions from an analytical classical model and nonequilibrium molecular dynamics simulations

Ganesh Balasubramanian,*[a] Ishwar K. Puri,[a] Michael C. Böhm[b] and Frédéric Leroy*[b]

We introduce an analytical model to rapidly determine the thermal conductivity reduction due to mass disorder in nanomaterials. Although this simplified classical model depends only on the masses of the different atoms, it adequately describes the changes in thermal transport as the concentrations of these atoms vary. Its predictions compare satisfactorily with nonequilibrium molecular dynamics simulations of the thermal conductivity of ^{14}C–^{12}C carbon nanotubes as well as with previous simulations of other materials. We present it as a simple tool to quantitatively estimate the thermal conductivity decrease that is induced by isotope substitution in various materials.

1. Introduction

There is a growing interest in fabricating materials for sustainable energy applications that have a high thermoelectric efficiency at room temperature,[1] *e.g.*, to generate electricity from waste heat. The thermoelectric properties of a material can be improved by suitably tailoring its structure at the nanometre scale. This strategy allows for a significant reduction in the thermal conductivity of a nanostructured thermoelectric as compared to bulk materials.[2,3] When the characteristic dimension of these nanostructures approaches the phonon mean free path, the resulting perturbations in the lattice vibrations (phonons) that enable heat transport are larger than the corresponding variations in the electrical conductivity. This understanding has led to the development of nanomaterials such as nanowires, superlattices and solid thin films that have much smaller thermal conductivities in comparison with their bulk counterparts.[4–8] Chemical modifications of nanomaterials can also significantly alter their magnetic properties.[9,10] While perturbation of the phonon propagation is generally caused by different scattering mechanisms,[11] phonon scattering in those materials mostly arises at the boundaries because of the large surface-to-volume ratio induced by the large extent of outer surface and interfaces.

Phonon scattering in silicon–germanium superlattice nanowires that have diameters of several tens of nanometres is dominated by atomic disorder (alloy scattering) rather than the surface scattering.[12] Thermal conductivity reduction through atomic disorder has been measured in various bulk materials including alloys and isotope mixtures.[13–20] Even a small mass difference in these materials significantly changes their heat transport properties. For example, a change in the ^{13}C isotope fraction from 0.07% to 1% in diamond can reduce the corresponding thermal conductivity by approximately 30%.[21] Therefore, we particularly consider the effects of mass disorder in nanostructured materials on the thermal conductivity as a strategy to reduce it.

This insight has motivated several recent molecular dynamics (MD) simulations and band structure calculations, which have sought to understand how heat transfer reduction occurs in nanomaterials. In accord with experimental measurements, their predictions show that surface roughness and porosity play an important role in controlling the thermal conductivity of silicon nanowires.[22–24] MD simulations predict that the introduction of either silicon isotopes or germanium into the material lattice induces a thermal conductivity decrease relative to a pure silicon nanowire.[25–28] Likewise, MD simulations of nanostructures with isotope defects also predict a thermal conductivity reduction in carbon based materials such as single walled carbon nanotubes (SWCNTs),[29,30] SWCNT superlattices,[31] graphene sheets[32] and nanoribbons.[33] Indeed, these show that the room temperature thermal conductivity can be reduced by almost an order of magnitude by simply doping the corresponding nanostructures with isotopes.

A theoretical framework for the heat transfer reduction that occurs due to mass disorder in lattices was defined more than fifty years ago by Klemens[34] and Callaway.[35] They showed that a point defect that is induced by a mass difference in a crystal lattice causes phonon scattering. Moreover, if this mass-induced

[a]Department of Engineering Science and Mechanics, Virginia Tech, 200 Norris Hall, Blacksburg, VA, 24061, USA. E-mail: bganesh@vt.edu; Fax: +1-540-231-4574; Tel: +1-540-231-4655

[b]Eduard-Zintl-Institut für Anorganische und Physikalische Chemie, Technische Universität Darmstadt, Petersenstrasse 20, 64287 Darmstadt, Germany. E-mail: f.leroy@theo.chemie-tu-darmstadt.de; Fax: +49 (0) 6151 16-6526; Tel: +49 (0)6151 16-6523

This journal is © The Royal Society of Chemistry 2011

scattering dominates the whole phonon scattering, the lattice thermal conductivity is driven by the masses and concentrations of the individual isotopes that contribute to the disorder. More recently, comprehensive theoretical tools have been employed to analyze and to predict the thermal conductivity of nano-structures, including those with mass disorder.[36–40] Despite the use of analytical methods and time-consuming computer simulations, a theoretical prescription that offers access to the heat transfer reduction on the basis of accessible input parameters is still missing.

In this paper, we present a simple classical model based on a mean-field approximation to evaluate the thermal conductivity variation in systems for which phonon scattering is induced through the presence of two different masses. The model requires only the masses of the different isotopes and their molar fractions, and does not contain adjustable parameters. It is able to correctly describe molecular dynamics predictions of the thermal conductivity reduction in solid nanomaterials of carbon upon isotope substitution. Reasonably good agreement is also observed between our model predictions and recently published MD results for silicon crystals[41] and silicon–germanium nanowires.[26] Since the model readily predicts the thermal conductivity changes due to isotope substitution in nanomaterials at room temperature without resorting to complex calculations, its capability is also of practical interest. It should be understood that a competition with the sophisticated theories mentioned above has not been the intention of our work.

We first present MD calculations of the classical density of vibrational states (DVS) of single walled armchair (10,10) carbon nanotubes containing different fractions of ^{12}C and ^{14}C isotopes at room temperature. Equipped with these results, we next introduce the classical model mentioned above. Finally, we validate the model using nonequilibrium MD simulations of ^{14}C isotope enriched CNTs and investigate its predictive ability by correlating our data with other MD results reported in the literature.

2. Theoretical background and methodology

Equilibrium molecular dynamics simulations

MD simulations of 40 nm long (10,10) CNTs consisting of 6520 atoms were performed using the LAMMPS code.[42] Periodic boundary conditions (PBCs) were applied in all directions so that the CNTs are essentially infinitely long in the z direction. The PBC applied along the z axis eliminates the effects of phonon-boundary scattering. The x and y dimensions of the simulation cell were large enough to prevent the tubes from interacting with their own periodic images in the lateral directions. Various fractions of ^{12}C atoms were randomly selected and replaced by ^{14}C isotopes. The Adaptive Intermolecular Reactive Empirical Bond Order (AIREBO) potential model was employed to reproduce the bonded interactions as well as the nonbonded interactions which are both of the attractive dispersion and of the repulsive type. They are mapped by a Lennard-Jones potential.[43,44] Each system was initialized at 300 K and simulated for 0.5 nanoseconds (ns) at 300 K and 1 atm (NPT ensemble). We employ the Nosé–Hoover thermostat and barostat, each with a coupling time of 100 femtoseconds (fs). This ensured that the

CNT was free of internal stresses and relaxed to its appropriate thermodynamic density. Next, the canonical (NVT) ensemble was imposed and the system relaxed at constant temperature and volume for 0.5 ns after which the equilibrated CNT structure was obtained. All simulations used 1 fs time steps.

Equilibrium simulations in the canonical ensemble at 300 K were used to calculate the classical DVS from the Fourier transform of the ensemble averaged mass weighted velocity auto-correlation function (VACF).[45] The equilibrated CNT structure was run for 1 ns with trajectories sampled every 100 ps. Each of these trajectories was independently simulated for 8.5 ps and the velocities were recorded every 1 fs. The time-translation invariance of the VACF was used to obtain a correlation over 8.192 ps by performing an average over 309 time origins. The average of all VACFs was Fourier transformed to obtain the DVS spectra with a 2.036 cm^{-1} resolution. In order to improve the signal-to-noise ratio of the Fourier transform, the VACFs were multiplied by an exponential function that had a characteristic decay time of 5 ps. Such a procedure is widely used in the treatment of the free induction decays in NMR spectroscopy.[46] This filtering function broadens the bands of the spectrum while appreciably decreasing the noise. Since the characteristic time was chosen to be close to the maximum time correlation of the VACFs, only a very slight broadening of the bands was observed.

Density of vibrational states analysis

The DVS spectra of the pure ^{12}C and ^{14}C nanotubes, as well as of a CNT with 40% of ^{14}C, are presented in Fig. 1a. The spectra of the systems that contain the ^{14}C isotope are shifted along the y-axis for clarity. The general shape of the spectra is in line with literature data.[47,48] The structure with two broad profiles below 700 cm^{-1} arises mainly from the radial vibration modes of the CNT.[49,50] The maximum around 1762 cm^{-1} in the pure
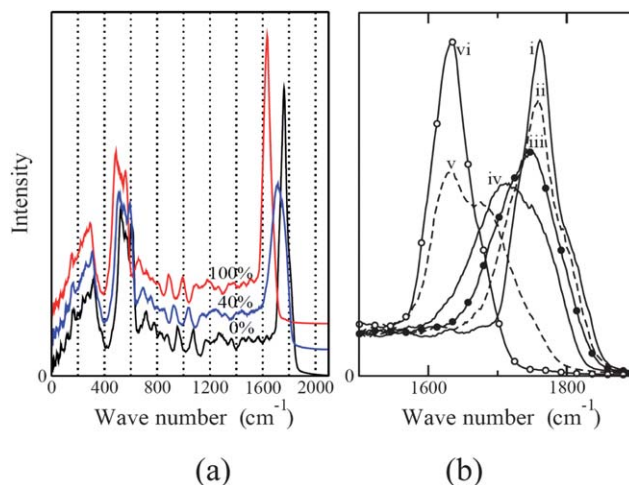

Fig. 1 (a) Density of vibrational states (DVS) of CNTs containing 0% (black), 40% (blue) and 100% (red) of the ^{14}C isotope, respectively. The spectra at 40% and 100% are displaced in the y direction in order to allow a convenient comparison. (b) DVS of the CNTs containing 0% (i), 10% (ii), 20% (iii), 40% (iv), 80% (v), and 100% (vi) of the ^{14}C isotope. The plot is restricted to the region between 1500 and 1900 cm^{-1}. The intensity in both plots is reported in arbitrary units.

^{12}C nanotube corresponds to the fastest vibrational modes in the system that can be associated with more or less localized stretching modes of the carbon atoms around their equilibrium position. The localized nature of these high energy modes can be deduced from calculations in the momentum space.[50] This boundary frequency can also be interpreted as the Einstein frequency of the CNT lattice, which corresponds to the frequency of an isolated atom vibrating in the potential energy surface generated by its local environment.

Fig. 1b shows that the high energy modes shift towards lower wave numbers when the ^{14}C content increases. The high energy maximum of the DVS for a pure ^{14}C nanotube occurs at 1632 cm^{-1}. The height of this peak decreases until the content of ^{14}C is around 50%, beyond which it increases again. This reduction correlates with a broadening of the high-energy DVS; it splits between 1762 and 1632 cm^{-1}. Thus, the results show that the local vibrational characteristics of a system with an intermediate content of isotopes are influenced by the mass disorder introduced in the network of atoms. While we have not presented the low frequency behavior of the DVS spectra in Fig. 1b for the sake of visual clarity, we have observed the wave number shift to be smaller in the low frequency region than at higher frequencies.

The high energy maximum in Fig. 1a and b for the two pure isotope CNTs corresponds to the more or less local modes described above. This can be illustrated through a simple model that predicts the change of the corresponding wave number when a system contains isotopes of different masses. In order to build this model, we compute the wave number of an isolated vibrating atom whose mass m_x is the average atomic mass in the system defined by

$$m_x = x m_\beta + (1-x) m_\alpha \qquad (1)$$

where m_α and m_β denote the masses of the two isotopes α and β, and x the molar fraction of isotope β that has substituted isotope α in the structure. In the harmonic approximation, the wave number depends on the square root of the product of the force constant and the inverse of the mass of the considered atom. Since the system consists of isotopes with a similar electronic structure that can be described adequately in the Born–Oppenheimer approximation, we neglect the change in the local curvature of the potential energy surface (which yields the force constant) induced by the mass difference. The ratio between the wave number v_0 at $x = 0$ and v_x for a specified fraction x of isotopes β is,

$$\frac{v_0}{v_x} = \sqrt{x \frac{m_\beta}{m_\alpha} + (1-x)} \qquad (2)$$

Fig. 2 presents the DVS spectra for systems with different contents of the ^{14}C isotope. The wave number axis of all the spectra is rescaled by the factor in eqn (2). The spectra are also shifted along the y-axis for visual ease. It can be seen that the major changes in the DVS spectra occur in the high energy region beyond 1600 cm^{-1}. Nevertheless, the high energy spectra in the two pure systems coincide when the rescaled wave numbers are used. Moreover, all the rescaled spectra are generally similar in the region below 1600 cm^{-1} (with small differences in the DVS structure that are beyond the scope of this work).
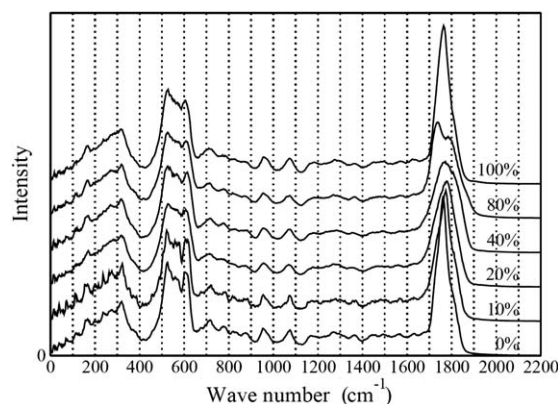

Fig. 2 Density of vibrational states (DVS) of CNTs containing 0%, 10%, 20%, 40%, 80% or 100% of the ^{14}C isotope. The wave numbers are rescaled according to eqn (2). The intensity in the plot is reported in arbitrary units.

The results show that approximately all the wave numbers in the system are influenced in a similar manner when ^{12}C is substituted by ^{14}C. This is consistent with the theoretical finding that the mass disorder dominates the changes in vibrational properties for classical systems at high temperature.[51] We can conclude from the DVS spectra that the vibrational states of the isotope substituted CNTs can be roughly approximated as a set of weakly coupled oscillators with wave numbers that are determined by the average atomic mass in the system. Although the employed rough estimate might imply that there is a monotonic variation in the thermal conductivity with respect to the isotope fraction, this variation is not monotonic, as will be shown later. The harmonic approximation employed in connection with eqn (2) should not be taken literally. It has only been used to estimate the mass dependence of the frequency shifts in the DVS spectra.

While energy transfer occurs through the vibrational modes of the system, the participation of the different modes can differ significantly.[23,52] Only the modes that are delocalized to a large extent can be expected to play an important role in heat conduction in crystal lattices. Even a small mass disorder is sufficient to prevent the formation of these perfectly delocalized modes that are most efficient for thermal transport. Thus, heat conduction is reduced by the presence of scattering sites created through mass disorder, *e.g.*, due to isotope substitution. We show in Fig. 1 and 2 that fingerprints of these changes also appear in the high energy region of the vibrational modes. While these findings might support interpretations highlighting the importance of the localized modes for the heat transport in nanomaterials, we believe that this picture neglects the changes in the phonon modes in the low energy range. In a recent MD study of CNTs adopting the Boltzmann transport equation, it has been shown that delocalized low energy modes (<700 cm^{-1}) account for most of the thermal conductivity,[23] which also agrees with our previous findings.[47]

A classical model based on mean-field approximation

Both experimental measurements of thermal conductivity and the corresponding results of MD simulations obtained from the

literature follow the typical features of Klemens' theory: (1) there is a substantial reduction in heat transfer upon isotope substitution even for materials with two isotopes that have similar masses, (2) the largest variation in the heat transfer reduction κ occurs for small isotope contents, (3) the maximum thermal resistance in binary systems occurs for an approximately equimolar mixture, and (4) a pure material made of the lightest isotope should have the highest thermal conductivity λ. Only the difference in mass and the mass defect molar fraction plays a central role in Klemens' theory. It can also be deduced from these observations that short-range modifications in the mass defect distribution are irrelevant to the reduction of heat transfer. This is illustrated by the frequency scaling of the DVS spectra described in Fig. 2. We conclude that a mean-field approximation for the mass distribution is applicable to map the isotope effect on the heat transfer reduction in isotope enriched CNTs.

In the mean-field approach, the heat transfer rate $\dot{Q}_x$ through an isotope enriched CNT is assumed to be proportional to the frequency ω_x of a single oscillator that is defined by two different bonded point masses $M_A(x)$ and $M_B(x)$. Thus, the heat transfer reduction is given by

$$\kappa(x) = \frac{\dot{Q}_x}{\dot{Q}_0} = \frac{\omega_x}{\omega_0} \quad (3)$$

M_A and M_B must depend linearly on the isotope fraction, such that $M_A = x M_\alpha$ and $M_B = (1-x) M_\beta$ to account for the variation in molar fraction with M_α and M_β denoting effective masses. In the harmonic approximation, the frequency of such an oscillator is inversely proportional to the square root of its reduced mass μ, where,

$$\frac{1}{\mu_x} = \frac{1}{x M_\beta} + \frac{1}{(1-x) M_\alpha} \quad (4)$$

The cases when the effective oscillator describes the homogeneous systems must be considered separately. An additional dimensionless parameter ε in eqn (5) ensures that the inverse reduced mass does not diverge in the limiting cases of $x = 0$ and $x = 1$. Hence,

$$\frac{1}{\mu_x} = \frac{1}{(x+\varepsilon) M_\beta} + \frac{1}{(1-x+\varepsilon) M_\alpha} \quad (5)$$

In order to establish the association between the frequency of an oscillator containing two atoms and the CNT thermal conductivity λ, we assume that it is the alteration in the heat transfer through the oscillator that reduces the thermal conductivity. Hence, the value for $\kappa(x)$ for a binary mixture in comparison with a pure ^{12}C nanotube is obtained from the change in the average frequency of the effective oscillator, which follows from eqn (5) as

$$\kappa(x) = \frac{\lambda(x)}{\lambda(0)} = \frac{\dot{Q}_x}{\dot{Q}_0} = \frac{\omega_x}{\omega_0} = \sqrt{\frac{\mu_0}{\mu_x}}$$

$$= \sqrt{\frac{\varepsilon(1+\varepsilon)[(1-x+\varepsilon)M_\alpha + (x+\varepsilon)M_\beta]}{(x+\varepsilon)(1-x+\varepsilon)[(1+\varepsilon)M_\alpha + \varepsilon M_\beta]}} \quad (6)$$

Eqn (6) is reminiscent of the factor in Klemens' theory[34,51] that quantifies the effect of isotope mass disorder on thermal conductivity. We will show that this equation is able to reproduce the features of that theory as enumerated above.

The three parameters M_α, M_β and ε in eqn (6) are numerically determined from considerations made on the systems of isotopes. Three values of κ can be identified on the basis of the following limiting cases. (1) Since κ is expected to predict the heat transfer reduction in comparison to a pure system containing the lightest isotope, $\kappa(0) = 1$ defines one limiting condition. (2) The second limiting case follows from our analysis of the DVS spectra: $\kappa(1) = (m_\beta/m_\alpha)^{-1/2}$. (3) The third value of κ is determined from the second situation where the local isotope distribution is approximately homogeneous. This is achieved when x is close to 0.5 for a mixture where isotopes are regularly distributed. In order to derive the reduction in the heat transfer rate in the vicinity of $x = 0.5$, we use the following mean-field construction. We assume that a pair of identical isotopes contributes constructively to energy transfer. On the contrary, two different isotopes are assumed to have a destructive effect. The contribution of a pair of bonded atoms to the heat transfer rate is inversely proportional to the square root of the reduced mass of the pair, which corresponds to $m_x/2$ when x is approximately 0.5. Finally, the average energy transfer rate σ_x at a specified isotope fraction x is obtained by adding the individual participations of each kind of possible pairs of bonded atoms. Each contribution is weighted by the probability that the given pair is found in the system so that,

$$\frac{\sigma_x}{\sigma_0} = \frac{\dot{Q}_x}{\dot{Q}_0} = \frac{1}{\sqrt{x(m_\beta/m_\alpha) + (1-x)}} \left[x^2 + (1-x)^2 - x(1-x) \right] \quad (7)$$

Eqn (7) considers that the probabilities for an oscillator to consist of two α-type isotopes and two β-type isotopes are approximately x^2 and $(1-x)^2$, respectively, whereas the probability that an oscillator is made of two different isotopes is approximately $x(1-x)$. This relation can be employed to derive the expression for the heat transfer reduction $\kappa(x) = \sigma_x/\sigma_0$. The constraints $\kappa(0) = 1$, $\kappa(1) = \sigma_1/\sigma_0$ and $\kappa(0.5) = \sigma_{0.5}/\sigma_0$ are used to numerically determine the complete set of parameters used in eqn (6).

Nonequilibrium molecular dynamics simulations

Reverse nonequilibrium molecular dynamics[53,54] (RNEMD) simulations were performed to probe the validity of the analytical model by computing the thermal conductivity of different CNTs. In RNEMD simulations, a steady heat flux is realized through the simulation cell by periodically imposing a kinetic energy exchange within specific regions of the system while the total energy and momentum are conserved. This imposed heat flux leads to a steady-state temperature gradient. Both the imposed heat flux and the measured temperature gradient are used to obtain the thermal conductivity from Fourier's law provided that the thermal gradient is linear, i.e. linear response holds. The RNEMD simulations were performed over the 5 ns that followed the equilibration described previously. The RNEMD velocity exchange period parameter covered 300 time steps. Temperatures and energy flux over the simulation cell were recorded every 1 ps, and a steady state was achieved by 3.5 ns. The last 1 ns of the simulation was used to determine the average thermal conductivity.

3. Results and discussion

The simulated values of λ for different fractions of ^{14}C isotope are reported in Table 1. The variation in the thermal conductivity

Table 1 Variation in the thermal conductivity of a (10,10) carbon nanotube with respect to the fraction of ^{14}C isotope at 300 K obtained from nonequilibrium molecular dynamics simulations. The error values reported here correspond to the standard errors computed from the different simulations.

Percentage of ^{14}C isotopes	Thermal conductivity λ/Wm^{-1} K^{-1}
0	173.16 $\pm$ 23.33
2.71	123.81 $\pm$ 11.57
5.24	85.60 $\pm$ 3.31
10.21	82.79 $\pm$ 2.92
12.63	79.55 $\pm$ 5.32
15.04	69.78 $\pm$ 3.26
20.53	63.65 $\pm$ 2.68
30.31	45.25 $\pm$ 1.67
40.82	38.51 $\pm$ 1.03
49.63	33.15 $\pm$ 0.73
60.06	41.53 $\pm$ 1.11
70.09	65.69 $\pm$ 3.04
79.65	74.32 $\pm$ 4.62
89.54	85.20 $\pm$ 5.21
100	114.83 $\pm$ 7.71

reduction factor $\kappa(x) = \lambda(x)/\lambda(0)$ upon isotope substitution is presented in Fig. 3. The observed nonmonotonic behavior is in agreement with Klemens' theory and has also been reported in other MD simulations.[27,29] The scatter in the MD results arises because a single calculation was used to obtain λ for each system. Averaging over a set of calculations with a different spatial isotope distribution should suppress such fluctuations.[30] Nevertheless, the simulation results are in very good agreement with the predictions from eqn (6) which are also reported in Fig. 3. The values of the model's parameters M_α, M_β and ε are reported in the caption of Fig. 3. The correlation between the model and the MD results clearly shows that changes in the short range order are irrelevant for the reduction in the thermal conductivity. It is rather the perturbation of the delocalized modes (*i.e.* long-range effect) that is responsible for the thermal conductivity changes.

The addition of ^{14}C reduces λ until the CNT contains approximately a 50% molar fraction of this isotope. Beyond this

fraction, the conductivity increases again with increasing substitution. For equimolar mixtures, the hindrance of delo-calized mode formation corresponds to a maximum. We furthermore compare the predictions of eqn (6) with MD simulations of the thermal conductivity of other carbon materials in Fig. 3. The model slightly overestimates λ for isotope substituted graphene nanoribbons,[33] but the overall agreement is still good. Our model is also able to predict $\kappa(x)$ for ^{13}C isotope substitution in graphene sheets.[32] Thus, the thermal conductivity behavior of isotope-substituted graphene is also well reproduced by eqn (6). Fig. 4a shows that eqn (6) is also able to predict the MD simulation results for the thermal conductivity of binary mixtures of ^{28}Si, ^{29}Si and ^{30}Si isotopes in silicon crystals.[41] This agreement seems to be an outcome of the very small differences between the masses of the isotopes. The values of M_α, M_β and ε corresponding to silicon isotope systems are reported in the caption of Fig. 4a.

However, the thermal conductivity reduction in a (5,5) CNT[29,30] is reproduced poorly by our model (not shown here). While the model predicts a maximum reduction of 75%, the simulations report a maximum reduction of 40% at most. We implicitly assume in the parameterization of our model that the scattering induced by the mass defects can be described through the stretching mode between two bonded atoms. However, for structures with large curvature like (5,5) CNTs it may be necessary to explicitly consider the coupling to bending or breathing modes to obtain a more precise description of the thermal transport.[50] The absence of such effects in a two-center model could explain the disagreement between its predictions and the mentioned results for (5,5) CNTs. Implications of coupling
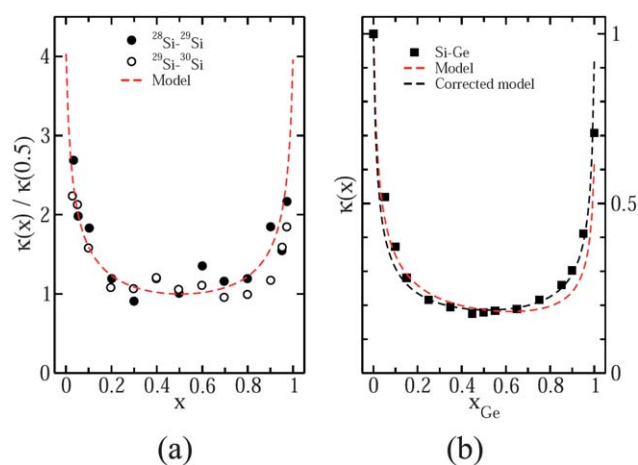
Fig. 4 (a) Comparison between the model and the MD simulations of silicon crystals[41] with ^{28}Si and ^{29}Si with ^{29}Si and ^{30}Si substitution, respectively. x denotes the fraction of the lightest isotope, *i.e.* ^{28}Si or ^{29}Si. The ratio $\kappa(x)/\kappa(0.5)$ is presented instead of $\kappa(x)$ because data for the pure components are unavailable. The dashed red line corresponds to our model of eqn (6) with $M_\alpha = 1.406$, $M_\beta = 1.356$ and $\varepsilon = 0.01639$. (b) Comparison between MD simulations in silicon–germanium nanowires[26] and the prediction of eqn (6). The dashed red line is obtained from constraints on σ in eqn (7) which yields $M_\alpha = 1.388$, $M_\beta = 0.5220$ and $\varepsilon = 0.01307$, while the dashed black line is obtained from constraints on the first derivative of σ; they lead to $M_\alpha = 1.072$, $M_\beta = 0.9256$ and $\varepsilon = 0.009558$.
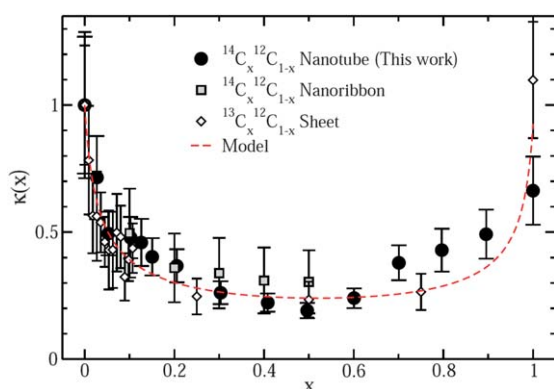
Fig. 3 Comparison between our RNEMD calculations (filled circles), the heat transfer reduction model (dashed line), and previous simulations for graphene nanoribbons[33] (open squares) and graphene sheets[32] (open diamonds). The values of the model's parameters are $M_\alpha = 1.393$, $M_\beta = 1.188$ and $\varepsilon = 0.01630$. x denotes the fraction of the lightest isotope.

effects of bonds over small CNT diameters have been commented in a recent study by some of the present authors.[47]

A comparison of the model with experimental measurements is difficult because of the lack of data. Measurements for ^{12}C enriched diamond are restricted to a very small amount of ^{13}C isotopes.[21] Such substitutions produce a reduction of approximately 30–36% in λ while our analytical model predicts a decrease of about 19% as the ^{13}C isotope fraction is varied from 0.07% to 1%. When the fraction of ^{13}C is varied from 0.5% to 1% in the experiments, there is a 6–12% reduction in the conductivity while our model predicts a decrease of 10%. The experimental trend is in qualitative agreement with the results obtained from simulations for carbon and silicon materials.

We also evaluate the applicability of our model for systems in which the difference between the masses exceeds that between two typical isotopes of the same element. Here, we choose different elements from the same group in the periodic table. Note that in contrast to isotope mixtures, element mixtures lead to increasing deviations from the potential energy surface of one component when the mole fraction of the other component is enhanced. However, we show that a slight modification of the parameterization of the model in eqn (6) is sufficient to keep the model's ability to predict the thermal conductivity reduction in those binary mixtures. Fig. 4b presents a comparison between our model predictions and earlier simulations of silicon–germanium nanowires.[26] The dashed red line in Fig. 4b is obtained from eqn (6) by constraining the values of $\kappa(0)$, $\kappa(1)$ and $\kappa(0.5)$ as described above. Although the results for a low germanium content are good, this procedure yields a result that contradicts the requirement of maximum thermal conductivity reduction (i.e. the minimum of κ) around $x = 0.5$, as can be seen from the distorted shape of the red curve in Fig. 4b. It is therefore more consistent to constrain the minimization of κ through its first derivative with respect to x. However, it is not possible to use the value of this derivative at $x = 0.5$ since it yields a symmetric variation in κ with respect to $x = 0.5$. Such mirror symmetry violates the constraint that the thermal conductivity of the lightest material should be larger than that of the heaviest. We therefore locate the minimum of κ at x_{min} for which the ratio σ_{xmin}/σ_0 obtained from eqn (7) is minimized. The new set of constraints is thus $\kappa(0) = 1$, $\kappa(x_{min}) = \sigma_{xmin}/\sigma_0$ and $d\kappa(x_{min})/dx = 0$. The model's parameters to which this procedure yields are reported in the caption of Fig. 4b. $\kappa(1)$ henceforth becomes an output of the model. The resulting variation of $\kappa(x)$, shown as the dashed black line in Fig. 4b, improves the agreement with the simulations. The variation of $\kappa(x)$ in Fig. 3 (carbon materials) and 4a (silicon crystals) is not modified by the new set of constraints. This is because the previously observed distorted shape arises due to the large mass difference between silicon and germanium, while isotope systems are characterized by very similar masses.

Our model is also in qualitative agreement with recent simulations of silicon–germanium core–shell nanowires.[28] This study found that germanium coatings reduce the thermal conductivity of silicon nanowires by 70–76%, which is similar to the maximum reduction predicted by our model in Fig. 4b. The molar fractions of germanium in that study are in line with those corresponding to the smallest values of κ in Fig. 4b. Furthermore, for a specified nanowire length, the thermal conductivity reduction for the Si/Ge composite in comparison with its uncoated silicon counterpart increases when the fraction of germanium increases. This trend is also predicted by our analytical model when the fraction of germanium is smaller than 50%. Finally, the reduction in thermal conductivity of the composite is somewhat insensitive to the nanowire length. This can also be explained with our model since increasing the nanowire length does not modify the ratio between silicon and germanium molar fractions. Therefore, the fraction of pairs of atoms which contribute either constructively or destructively to heat transfer remains the same.

Admittedly, there are limitations to the above approach. The model describes disordered structures without accounting for the long-range order in the arrangement of the mass defects. Nevertheless, the qualitative agreement of the model with MD simulations of silicon–germanium nanowires suggests that it might also be applicable for ordered structures. The implication is that the mass difference between atoms would then represent the major contribution to heat transfer perturbations regardless of the precise arrangement of atoms. We anticipate future MD simulations that are accompanied by calculations of phonon dispersion and electronic properties in the momentum space that will more fully characterize the degree of ordering that the model is able to describe.

4. Conclusion

We have derived a simple model that predicts the reduction in heat conduction due to isotope substitution and mass disorder in binary solid materials. The model which is purely classical and based on effective harmonic oscillator properties depends only on the masses of the isotopes. Our objective is twofold: (1) on the one hand, we aim to propose a tool that readily provides acceptable results rather than competing with more detailed theories, and (2) on the other hand, we show that a mean-field approximation is applicable to the description of heat transfer in solid nanomaterials. While the model should be used with caution at low temperatures when quantum effects are likely to play a role, it is possible to decouple the temperature effect from the mass disorder effect.[51] In this case, the effect of temperature can be subsequently included as a multiplying factor.

Acknowledgements

References

1 G. J. Snyder and E. S. Toberer, Nat. Mater., 2008, 7, 105–114.
2 J. K. Yu, S. Mitrovic, D. Tham, J. Varghese and J. R. Heath, Nat. Nanotechnol., 2010, 5, 718–721.
3 G. Galli and D. Donadio, Nat. Nanotechnol., 2010, 5, 701–702.
4 R. Venkatasubramanian, E. Siivola, T. Colpitts and B. O'Quinn, Nature, 2001, 413, 597–602.
5 A. I. Boukai, Y. Bunimovich, J. Tahir-Kheli, J. K. Yu, W. A. Goddard and J. R. Heath, Nature, 2008, 451, 168–171.

6 A. I. Hochbaum, R. K. Chen, R. D. Delgado, W. J. Liang, E. C. Garnett, M. Najarian, A. Majumdar and P. D. Yang, *Nature*, 2008, **451**, 163–167.
7 J. Y. Tang, H. T. Wang, D. H. Lee, M. Fardy, Z. Y. Huo, T. P. Russell and P. D. Yang, *Nano Lett.*, 2010, **10**, 4279–4283.
8 G. Pernot, M. Stoffel, I. Savic, F. Pezzoli, P. Chen, G. Savelli, A. Jacquot, J. Schumann, U. Denker, I. Monch, C. Deneke, O. G. Schmidt, J. M. Rampnoux, S. Wang, M. Plissonnier, A. Rastelli, S. Dilhaire and N. Mingo, *Nat. Mater.*, 2010, **9**, 491–495.
9 M. Wang and C. M. Li, *New J. Phys.*, 2010, **12**, 083040.
10 M. Wang and C. M. Li, *Phys. Chem. Chem. Phys.*, 2011, **13**, 5945–5951.
11 N. W. Ashcroft and N. D. Mermin, *Solid State Physics*, Holt, Rinehart and Winston, New York, 1976.
12 D. Y. Li, Y. Wu, R. Fan, P. D. Yang and A. Majumdar, *Appl. Phys. Lett.*, 2003, **83**, 3186–3188.
13 A. V. Inyushkin, *Inorg. Mater.*, 2002, **38**, 427–433.
14 V. G. Plekhanov, *Phys.-Usp.*, 2003, **46**, 689–715.
15 D. T. Morelli, J. P. Heremans and G. A. Slack, *Phys. Rev. B: Condens. Matter Mater. Phys.*, 2002, **66**, 195304.
16 T. H. Geballe and G. W. Hull, *Phys. Rev.*, 1958, **110**, 773–775.
17 R. K. Kremer, K. Graf, M. Cardona, G. G. Devyatykh, A. V. Gusev, A. M. Gibin, A. Inyushkin, A. Taldenkov and H. J. Pohl, *Solid State Commun.*, 2004, **131**, 499–503.
18 D. G. Cahill and F. Watanabe, *Phys. Rev. B: Condens. Matter Mater. Phys.*, 2004, **70**, 235322.
19 C. W. Chang, A. M. Fennimore, A. Afanasiev, D. Okawa, T. Ikuno, H. Garcia, D. Y. Li, A. Majumdar and A. Zettl, *Phys. Rev. Lett.*, 2006, **97**, 085901.
20 J. P. Dismukes, E. Ekstrom, E. F. Steigmeier, I. Kudman and D. S. Beers, *J. Appl. Phys.*, 1964, **35**, 2899–2907.
21 T. R. Anthony, W. F. Banholzer, J. F. Fleischer, L. H. Wei, P. K. Kuo, R. L. Thomas and R. W. Pryor, *Phys. Rev. B: Condens. Matter Mater. Phys.*, 1990, **42**, 1104–1111.
22 J. H. Lee, G. A. Galli and J. C. Grossman, *Nano Lett.*, 2008, **8**, 3750–3754.
23 D. Donadio and G. Galli, *Phys. Rev. Lett.*, 2009, **102**, 195901.
24 J. Chen, G. Zhang and B. W. Li, *Nano Lett.*, 2010, **10**, 3978–3983.
25 N. Yang, G. Zhang and B. W. Li, *Nano Lett.*, 2008, **8**, 276–280.
26 J. Chen, G. Zhang and B. W. Li, *Appl. Phys. Lett.*, 2009, **95**, 073117.
27 G. Zhang and B. W. Li, *Nanoscale*, 2010, **2**, 1058–1068.
28 M. Hu, K. P. Giapis, J. V. Goicochea, X. Zhang and D. Poulikakos, *Nano Lett.*, 2011, **11**, 618–623.
29 S. Maruyama, Y. Igarashi, Y. Taniguchi and J. Shiomi, *J. Therm. Sci. Technol.*, 2006, **1**, 138–148.
30 G. Zhang and B. W. Li, *J. Chem. Phys.*, 2005, **123**, 114714.
31 J. Shiomi and S. Maruyama, *Phys. Rev. B: Condens. Matter Mater. Phys.*, 2006, **74**, 155401.
32 H. Zhang, G. Lee, A. F. Fonseca, T. L. Borders and K. Cho, *J. Nanomater.*, 2010, **2010**, 537657.
33 J. W. Jiang, J. H. Lan, J. S. Wang and B. W. Li, *J. Appl. Phys.*, 2010, **107**, 054314.
34 P. G. Klemens, *Proc. Phys. Soc., London, Sect. A*, 1955, **68**, 1113–1128.
35 J. Callaway, *Phys. Rev.*, 1959, **113**, 1046–1051.
36 P. Chantrenne, J. L. Barrat, X. Blase and J. D. Gale, *J. Appl. Phys.*, 2005, **97**, 104318.
37 N. Mingo, D. A. Stewart, D. A. Broido and D. Srivastava, *Phys. Rev. B: Condens. Matter Mater. Phys.*, 2008, **77**, 033418.
38 I. Savic, N. Mingo and D. A. Stewart, *Phys. Rev. Lett.*, 2008, **101**, 165502.
39 D. A. Stewart, I. Savic and N. Mingo, *Nano Lett.*, 2009, **9**, 81–84.
40 M. Kazan, G. Guisbiers, S. Pereira, M. R. Correia, P. Masri, A. Bruyant, S. Volz and P. Royer, *J. Appl. Phys.*, 2010, **107**, 083503.
41 A. Murakawa, H. Ishii and K. Kakimoto, *J. Cryst. Growth*, 2004, **267**, 452–457.
42 S. Plimpton, *J. Comput. Phys.*, 1995, **117**, 1–19.
43 D. W. Brenner, O. A. Shenderova, J. A. Harrison, S. J. Stuart, B. Ni and S. B. Sinnott, *J. Phys.: Condens. Matter*, 2002, **14**, 783–802.
44 S. J. Stuart, A. B. Tutein and J. A. Harrison, *J. Chem. Phys.*, 2000, **112**, 6472–6486.
45 H. Jobic, K. S. Smirnov and D. Bougeard, *Chem. Phys. Lett.*, 2001, **344**, 147–153.
46 J. Keeler, *Understanding NMR spectroscopy*, John Wiley and Sons Ltd., The Atrium, 2005.
47 M. Alaghemandi, J. Schulte, F. Leroy, F. Müller-Plathe and M. C. Böhm, *J. Comput. Chem.*, 2011, **32**, 121–133.
48 C. Ren, W. Zhang, Z. Xu, Z. Zhu and P. Huai, *J. Phys. Chem. C*, 2010, **114**, 5786–5791.
49 A. M. Rao, E. Richter, S. Bandow, B. Chase, P. C. Eklund, K. A. Williams, S. Fang, K. R. Subbaswamy, M. Menon, A. Thess, R. E. Smalley, G. Dresselhaus and M. S. Dresselhaus, *Science*, 1997, **275**, 187–191.
50 D. Sanchez-Portal, E. Artacho, J. M. Soler, A. Rubio and P. Ordejon, *Phys. Rev. B: Condens. Matter Mater. Phys.*, 1999, **59**, 12678–12688.
51 P. G. Klemens, *Phys. Rev.*, 1960, **119**, 507–509.
52 Z. W. Tan, J.-S. Wang and C. K. Gan, *Nano Lett.*, 2011, **11**, 214–219.
53 F. Müller-Plathe, *J. Chem. Phys.*, 1997, **106**, 6082–6085.
54 M. Alaghemandi, E. Algaer, M. C. Böhm and F. Müller-Plathe, *Nanotechnology*, 2009, **20**, 115704.